PERGAMON

International Journal of Solids and Structures 40 (2003) 7035–7053

INTERNATIONAL JOURNAL OF SOLIDS and STRUCTURES

www.elsevier.com/locate/ijsolstr

Analysis of progressive fiber debonding in elastic laminates

Yehia A. Bahei-El-Din [a,*], Amany G. Botrous [b]

[a] *Department of Mechanical and Aerospace Engineering, North Carolina State University, College of Engineering, Campus Box 7910, 3211, Broughton Hall, Raleigh, NC 27695-7910, USA*

[b] *Department of Civil Engineering, Tanta University, Tanta, Egypt*

Received 21 October 2002

Abstract

The evolution of fiber debonding, and sliding, in fibrous laminates is modeled by a coupled micro/macro-mechanical analysis scheme. The laminates under consideration have a symmetric layup, and are subjected to mechanical loads. The individual plies are elastic, have a unidirectional reinforcement, and can suffer local damage at the fiber/matrix interface when the resolved normal and shear stresses exceed their ultimate magnitudes. The local fields in the plies are assumed to be periodic, and are approximated by the finite element method for overall loads and local resolved stresses that are in excess of the interface strength. Local effects in the individual plies are scaled up to the laminate analysis through stress transformation factors, which are a function of the elastic properties of the plies and their stacking configuration.

The proposed analysis was implemented for a periodic array model of the laminas, and for in-plane loading of the laminate. The model predictions for a unidirectional steel/epoxy system subjected to transverse loading compare remarkably well with experimental measurements. This result, and several other examples given for axial and off-axis loading of SiC/CAS laminates, illustrate the model capabilities in predicting the overall strains in the presence of simultaneous, progressive debonding in the individual plies.

Keywords: Laminate mechanics; Micromechanics; Debonding; Analytical modeling; Finite element analysis

1. Introduction

Material interfaces present in composite aggregates have a profound effect on the local fields and on the overall behavior. Weak or debonded interfacial regions cause redistribution of the local stresses, which generally enhances the overall compliance. This is manifested in the measured overall response of elastic, fibrous composite systems under transverse tensile stress (Ghosh et al., 2000; Tandon et al., 2000), and under shear stress (Wooh and Daniel, 1994). In general, a knee in the overall stress–strain response, which is otherwise linear, and a reduced overall stiffness characterize the onset of fiber debonding or sliding. The debonded regions propagate along the fiber interface under subsequent loading, which leads to further reductions in the overall stiffness. A constant value is eventually measured for the overall moduli, which is indicative of local damage saturation.

* Corresponding author. Tel.: +1-919-515-2365; fax: +1-919-515-7968.
E-mail address: yabaheie@unity.ncsu.edu (Y.A. Bahei-El-Din).

0020-7683/$ - see front matter © 2003 Elsevier Ltd. All rights reserved.
doi:10.1016/S0020-7683(03)00353-6

Several publications have been devoted to describing initiation and propagation of fiber debonding in unidirectional composites, both experimentally and analytically. Examples are found in the work of Evans et al. (1989), Hsueh and Becher (1998), Hutchinson and Jensen (1990), Liu and Kagawa (1996), Marshall (1992), Mumm and Faber (1995), Pochiraju et al. (2001), Steif and Dollar (1992), and Zhou et al. (1999), among many others. Since the objective was to understand and characterize this phenomenon, the focus has been on the local, interfacial behavior. The effect of fiber debonding on certain overall moduli of a unidirectional composite has also been the subject of several publications, among which is the work of Dvorak and Zhang (2001), Nimmer et al. (1991), Shan and Chou (1995), and Steif and Dollar (1988). The information obtained from these studies is invaluable in describing the local debonding event and its repercussion on the overall behavior, and in providing mechanical properties, such as the interface strength magnitudes and the decay in overall moduli.

Modeling the overall behavior of unidirectional fibrous systems in the presence of local interface damage under specific loading regimes, however, cannot be utilized in composite structures, such as laminates, since the lamina loading path is not known a priori. Instead, the problem needs to be analyzed under a general stress or strain state, which follows a general regime, such that it can be included in a hierarchical analysis for composite structures. On the other hand, analytical characterization of the overall behavior of laminated structures, as macroscopically homogeneous, anisotropic materials with local interface damage is not feasible since the local fields are not known.

This paper describes an analytical approach for predicting the overall response of symmetric fibrous laminates under overall in-plane loads and local fiber debonding. The model is a coupled micro/macromechanical analysis scheme with closed form equations developed for the laminate, and a finite element analysis performed for the individual plies. The latter assumes a periodic dispersion of elastic fibers in an elastic matrix, and replaces the local fields in a representative volume element (RVE) by a piecewise uniform approximation. Fiber debonding and sliding is examined in terms of the stresses in the matrix, averaged over small volumes adjacent to the fiber boundary. Stress transformation factors, which depend on the elastic properties of the plies and their stacking configuration, scale these local effects up to the laminate. A two-phase, fully debonded, averaging material model representing the unidirectional plies was also implemented in the proposed method for comparison with the finite element results. This paper is organized as follows: analysis of a unidirectional fibrous lamina, with progressive fiber debonding is described in Section 2, and analysis of symmetric laminates is given in Section 3. Results, which illustrate the model predictions for unidirectional composites and laminates are given in Section 4, including a comparison with experiments. The paper concludes with a closure in Section 5, which summarizes the work performed and discusses related issues that can benefit from future research.

The notation used here are symbolic, where symmetric second-order tensors are written as (6×1) matrices and denoted by boldface, lower case letters, and symmetric fourth-order tensors are written as (6×6) matrices and denoted by boldface, upper case letters. Connections with tensor notation are easily established. For example, the stress tensor σ_{ij}, and strain tensor ε_{ij}, with the symmetry $\sigma_{ij}=\sigma_{ji}$ and $\varepsilon_{ij}=\varepsilon_{ji}$, are written in a matrix form as $\boldsymbol{\sigma}=[\sigma_{11},\sigma_{22},\sigma_{33},\sigma_{23},\sigma_{31},\sigma_{12}]$, and $\boldsymbol{\varepsilon}=[\varepsilon_{11},\varepsilon_{22},\varepsilon_{33},2\varepsilon_{23},2\varepsilon_{31},2\varepsilon_{12}]$. Similarly, fourth-order tensors having at least the symmetries $A_{ijkl}=A_{jikl}=A_{ijlk}$ are reduced to (6×6) matrices $\mathbf{A}$, such that $\mathbf{A}\mathbf{A}^{-1}=\mathbf{A}^{-1}\mathbf{A}=\mathbf{I}$, the identity matrix.

2. Analysis of a unidirectional lamina

2.1. Constitutive equations

A volume V of the composite aggregate is selected such that it is representative of the fibrous lamina under consideration. The local stresses and strains within V vary pointwise, but will be approximated by

piecewise uniform fields over subvolumes V_r, $r = 1, 2, \ldots, Q$, such that $V = \sum V_r$, or $\sum c_r = 1$, where $c_r = V_r/V$ is the volume fraction. The number of subvolumes Q may be as small as two; one belongs to the matrix and the other to the fiber, as approximated for example by the averaging models. On the other hand, the fiber and matrix can be subdivided into many small volumes, which reside in either phase as employed, for example, in finite element modeling of the representative volume V. Let $\dot{\boldsymbol{\sigma}}_r$ and $\dot{\boldsymbol{\varepsilon}}_r$ denote time rates of stress and strain volume averages in a subvolume, and $\dot{\bar{\boldsymbol{\sigma}}}$ and $\dot{\bar{\boldsymbol{\varepsilon}}}$ denote uniform overall stress and strain rates in the material principal coordinates $\bar{\mathbf{x}}$ of the lamina. Then

$$\dot{\bar{\boldsymbol{\sigma}}} = \sum_{r=1}^{Q} c_r \dot{\boldsymbol{\sigma}}_r, \quad \dot{\bar{\boldsymbol{\varepsilon}}} = \sum_{r=1}^{Q} c_r \dot{\boldsymbol{\varepsilon}}_r. \tag{1}$$

Constitutive equations of the phases or subvolumes subjected to $\dot{\boldsymbol{\varepsilon}}_r$, or $\dot{\boldsymbol{\sigma}}_r$, and simultaneously undergoing uniform transformation strain $\dot{\boldsymbol{\mu}}_r$, or stress $\dot{\boldsymbol{\lambda}}_r$ are written as

$$\dot{\boldsymbol{\sigma}}_r = \mathbf{L}_r \dot{\boldsymbol{\varepsilon}}_r + \dot{\boldsymbol{\lambda}}_r, \quad \dot{\boldsymbol{\varepsilon}}_r = \mathbf{M}_r \dot{\boldsymbol{\sigma}}_r + \dot{\boldsymbol{\mu}}_r, \tag{2}$$

where $\mathbf{L}_r$ and $\mathbf{M}_r = \mathbf{L}_r^{-1}$ are elastic stiffness and compliance. From Eq. (2), the transformation stress and strain are related by $\dot{\boldsymbol{\lambda}}_r = -\mathbf{L}_r \dot{\boldsymbol{\mu}}_r$.

Similarly, the constitutive equations for the composite aggregate subjected to overall uniform strain $\dot{\bar{\boldsymbol{\varepsilon}}}$, or stress $\dot{\bar{\boldsymbol{\sigma}}}$, and undergoing uniform transformation strain $\dot{\bar{\boldsymbol{\mu}}}$, or stress $\dot{\bar{\boldsymbol{\lambda}}}$, are written as

$$\dot{\bar{\boldsymbol{\sigma}}} = \overline{\mathbf{L}} \dot{\bar{\boldsymbol{\varepsilon}}} + \dot{\bar{\boldsymbol{\lambda}}}, \quad \dot{\bar{\boldsymbol{\varepsilon}}} = \overline{\mathbf{M}} \dot{\bar{\boldsymbol{\sigma}}} + \dot{\bar{\boldsymbol{\mu}}}, \tag{3}$$

where $\overline{\mathbf{L}}$ and $\overline{\mathbf{M}} = \overline{\mathbf{L}}^{-1}$ are overall elastic stiffness and compliance matrices, and $\dot{\bar{\boldsymbol{\mu}}}$ and $\dot{\bar{\boldsymbol{\lambda}}}$ are related by $\dot{\bar{\boldsymbol{\lambda}}} = -\overline{\mathbf{L}} \dot{\bar{\boldsymbol{\mu}}}$.

The connection between the local strain and stress fields and their overall counterparts are found by superposition of mechanical and transformation field contributions (Dvorak, 1992),

$$\dot{\boldsymbol{\varepsilon}}_r = \mathbf{A}_r \dot{\bar{\boldsymbol{\varepsilon}}} + \sum_{s=1}^{Q} \mathbf{D}_{rs} \dot{\boldsymbol{\mu}}_s, \quad \dot{\boldsymbol{\sigma}}_r = \mathbf{B}_r \dot{\bar{\boldsymbol{\sigma}}} + \sum_{s=1}^{Q} \mathbf{F}_{rs} \dot{\boldsymbol{\lambda}}_s, \tag{4}$$

where $\mathbf{A}_r$ and $\mathbf{B}_r$ represent strain and stress concentration factors for the phase or subvolume (Hill, 1963, 1965), and $\mathbf{D}_{rs}$ and $\mathbf{F}_{rs}$ are transformation influence functions. Both the concentration factors and the influence functions depend on the microgeometry of the composite aggregate and elastic moduli of the phases, and are determined from a micromechanical model.

If the concentration factors $\mathbf{A}_r$ and $\mathbf{B}_r$ are known, one can find from Eqs. (1)–(4), in the absence of transformation fields, the overall elastic stiffness and compliance in the form

$$\overline{\mathbf{L}} = \sum_{r=1}^{Q} c_r \mathbf{L}_r \mathbf{A}_r, \quad \overline{\mathbf{M}} = \sum_{r=1}^{Q} c_r \mathbf{M}_r \mathbf{B}_r. \tag{5}$$

The transformation stress and strain are given in terms of their local counterparts by the generalized Levin's (1967) formula (Dvorak and Benveniste, 1992),

$$\dot{\bar{\boldsymbol{\lambda}}} = \sum_{r=1}^{Q} c_r \mathbf{A}_r^{\mathrm{T}} \dot{\boldsymbol{\lambda}}_r, \quad \dot{\bar{\boldsymbol{\mu}}} = \sum_{r=1}^{Q} c_r \mathbf{B}_r^{\mathrm{T}} \dot{\boldsymbol{\mu}}_r. \tag{6}$$

2.2. Local damage

Consider discrete damage in the phases or subvolumes that is characterized by loss of certain stiffness coefficients. The onset of damage is determined by in situ damage criteria. One such criterion is fiber

debonding, which is considered in Section 2.3. Our objective here is to describe how the stresses released in the damaged subvolumes are distributed in the lamina such that stress equilibrium is maintained.

Let t^* denote the time which signals the onset of damage in Q^* subvolumes, where $Q^* < Q$, and $\boldsymbol{\sigma}_\rho(t^*)$, $\rho = 1, 2, \ldots, Q^*$, denote the accumulated stresses found at time t^* in this group of subvolumes. Certain stress tractions caused by $\boldsymbol{\sigma}_\rho(t^*)$, but resolved into the free surfaces created for example by fiber debonding, must now be released and redistributed. Let $\hat{\boldsymbol{\sigma}}_\rho$ denote the released stresses in element V_ρ referred to the lamina coordinate system $\bar{x}_j$, $j = 1, 2, 3$. These are written in terms of the accumulated stress $\boldsymbol{\sigma}_\rho(t^*)$ as

$$\hat{\boldsymbol{\sigma}}_\rho = -\boldsymbol{\Phi}_\rho \boldsymbol{\sigma}_\rho(t^*). \tag{7}$$

The form of matrix $\boldsymbol{\Phi}_\rho$ depends on the micromechanical model of the composite aggregate and the local damage criterion. Specific forms are given in Section 2.3.

For each subvolume V_ρ, $\rho = 1, 2, \ldots, Q^*$, with local damage, the elastic stiffness $\mathbf{L}_\rho$ is modified to reflect the effect of damage on the elastic response. Generation of the reduced stiffness matrix, denoted by $\mathbf{L}^*_\rho$, is provided in Section 2.3. Next, new concentration factors $\mathbf{A}^*_r$, $\mathbf{B}^*_r$, and influence functions $\mathbf{D}^*_{rs}$, $\mathbf{F}^*_{rs}$, $r, s = 1, 2, \ldots, Q$, are computed with the micromechanical model of the lamina to reflect the changes in local stiffness.

At the onset of damage $t = t^*$, stress release from the damaged elements and their subsequent distribution within V is assumed to be instantaneous while the overall load is held constant. Hence at $t = t^{*+}$, immediately after the onset of damage, there is $\dot{\bar{\boldsymbol{\sigma}}} = \mathbf{0}$, and the transformation stresses in the subvolumes are given by (7). Substituting into $(4)_2$, the local stresses caused instantaneously in V_r, $r = 1, 2, \ldots, Q$, by the inception of damage in V_ρ, $\rho = 1, 2, \ldots, Q^*$, are obtained, and the accumulated stress at $t = t^*$ is modified as

$$\boldsymbol{\sigma}_r(t^{*+}) = \boldsymbol{\sigma}_r(t^*) - \sum_{\rho=1}^{Q^*} \mathbf{F}^*_{r\rho} \boldsymbol{\Phi}_\rho \boldsymbol{\sigma}_\rho(t^*). \tag{8}$$

Clearly, damage may develop in new subvolumes as a result of the stresses induced by (8). Upon evaluation of the local stresses by Eq. (8), the local damage criteria must be re-examined, and the stresses released from newly damaged subvolumes, if any, are redistributed. This process is repeated until damage saturation is reached at the current time $t = t^*$. Whenever new subvolumes show damage, their elastic stiffness is modified and the stress concentration factor and influence coefficient are recalculated. The latter is denoted by $\mathbf{F}^*_{r\rho}$ in Eq. (8).

2.3. Micromechanical models with simulated fiber debonding

2.3.1. Two-phase averaging models

This class of models centers on Eshelby's solution (Eshelby, 1957) of an ellipsoidal inhomogeneity in an infinite matrix under remotely applied uniform fields, to estimate the average stresses and strains in the fiber (f) and the matrix (m) and hence the stress and strain concentration factors $\mathbf{A}_r$, $\mathbf{B}_r$, $r = f, m$. In this case, the number of subdivisions of the representative volume V is $Q = 2$, as depicted in Fig. 1a, with V_r, $r = f, m$, denoting volume of the fiber and matrix phases, and c_f, c_m their volume fractions. The overall elastic stiffness and compliance are then found from Eq. (5). If on the other hand, the overall elastic moduli are known, by experimental measurements for example, the concentration factors can be found in closed form as (Hill, 1963)

$$\mathbf{A}_r = (\mathbf{L}_r - \mathbf{L}_s)^{-1}\big(\overline{\mathbf{L}} - \mathbf{L}_s\big)/c_r, \quad \mathbf{B}_r = (\mathbf{M}_r - \mathbf{M}_s)^{-1}\big(\overline{\mathbf{M}} - \mathbf{M}_s\big)/c_r, \quad r, s = f, m. \tag{9}$$

In any case, the influence coefficients are written in terms of the concentration factors and the phase elastic moduli as (Dvorak, 1991)

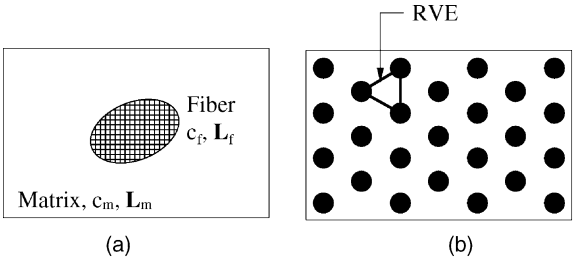

Fig. 1. Schematic of micromechanical models of a fibrous composite, (a) averaging model, and (b) periodic hexagonal array model.

$$\mathbf{D}_{rf} = (\mathbf{I} - \mathbf{A}_r)(\mathbf{L}_f - \mathbf{L}_m)^{-1}\mathbf{L}_f, \quad \mathbf{D}_{rm} = -(\mathbf{I} - \mathbf{A}_r)(\mathbf{L}_f - \mathbf{L}_m)^{-1}\mathbf{L}_m, \tag{10}$$

$$\mathbf{F}_{rf} = (\mathbf{I} - \mathbf{B}_r)(\mathbf{M}_f - \mathbf{M}_m)^{-1}\mathbf{M}_f, \quad \mathbf{F}_{rm} = -(\mathbf{I} - \mathbf{B}_r)(\mathbf{M}_f - \mathbf{M}_m)^{-1}\mathbf{M}_m, \quad r = f, m. \tag{11}$$

Estimates of the overall moduli provided by the Mori–Tanaka averaging model (Mori and Tanaka, 1973; Benveniste, 1987) are given in Appendix A.

Consider local damage in the form of debonding and/or sliding along the fiber/matrix interface. In principle, partial debonding of a single fiber from the surrounding matrix can be characterized since Eshelby's solution provides details of the matrix stress at the vicinity of the fiber interface. On the other hand, progressive debonding which involves several interacting fibers is a more difficult problem (Dvorak and Zhang, 2001). In the present work, assessment of damage at the fiber interface was based on the magnitude of the local field averages given by the Mori–Tanaka model. Consequently, debonding, or sliding, is assumed to take place along the entire circumference of the fiber interface when the maximum stresses resolved at the fiber circular boundary reach their respective ultimate values. The solution of the inclusion problem under certain overall stress, or strain, components which promote debonding or sliding therefore becomes that of a matrix containing a cavity that has the same shape as the fiber. In this case, we have $\boldsymbol{\sigma}_\rho(t^*) = \boldsymbol{\sigma}_f(t^*)$, the fiber stress found at the onset of damage.

Since the fiber stress is uniform, the resolved interface radial and shear stresses are computed as the principal, transverse normal and shear stresses in the fiber. Let the $\bar{x}_1$-axis be aligned with the fiber longitudinal axis and $\bar{x}_1\bar{x}_2$ is the transverse plane. Then, the onset of fiber sliding or debonding in the transverse plane is characterized, respectively, by

$$\sigma_{RT} \equiv \left(\frac{1}{4}\left(\sigma_{22}^f - \sigma_{33}^f\right)^2 + \left(\sigma_{23}^f\right)^2\right)^{1/2} = \tau_{ult} \quad \text{or} \quad \sigma_{RR} \equiv \frac{1}{2}\left(\sigma_{22}^f + \sigma_{33}^f\right) + \sigma_{RT} = \sigma_{ult}, \tag{12}$$

where σ_{RR} is the maximum principal stress and σ_{RT} is the maximum shear stress in the transverse plane, σ_{ult} is the interface normal bond strength, and τ_{ult} is the shear bond strength. Separation of the fiber and matrix under these conditions creates a stress-free interface. Under the uniform stress present in the fiber, a stress-free interface is modeled by vanishing the fiber transverse Young's modulus and shear modulus, $E_T^f = G_T^f = 0$ (Bahei-El-Din, 1996). The fiber stresses released in this case are the transverse normal and shear stresses. Hence matrix $\boldsymbol{\Phi}_\rho$, $\rho = f$, in Eq. (7) is a diagonal matrix with $\Phi_{22} = \Phi_{33} = \Phi_{44} = 1$, $\Phi_{11} = \Phi_{55} = \Phi_{66} = 0$.

Sliding along the fiber meridians occurs when the fiber longitudinal shear stress σ_{31}^f or σ_{12}^f, attains the interface ultimate shear strength τ_{ult}. In this case, the longitudinal shear modulus of the fiber vanishes, $G_L^f = 0$. Hence, $\Phi_{55} = \Phi_{66} = 1$, $\Phi_{11} = \Phi_{22} = \Phi_{33} = \Phi_{44} = 0$.

Under these circumstances, the reduced stiffness matrix of the fiber $\mathbf{L}_f^*$ is singular and the compliance $\mathbf{M}_f^*$ does not exist. However, the stress concentration factors $\mathbf{A}_r^*$, and the strain transformation influence coefficients $\mathbf{D}_{rf}^*$, $\mathbf{D}_{rm}^*$, $r = f, m$, can still be computed from Eqs. $(9)_1$ and (10). Computing the corresponding

stress concentration and influence coefficients, on the other hand, cannot be achieved with Eqs. $(9)_2$. Instead, the following equivalent equations are used (Bahei-El-Din, 1996)

$$\mathbf{B}_r = \mathbf{L}_r\mathbf{A}_r\overline{\mathbf{M}}, \quad \mathbf{F}_{rf} = (\mathbf{I}-\mathbf{B}_r)(\mathbf{I}-\mathbf{L}_f\mathbf{M}_m)^{-1}, \quad \mathbf{F}_{rm} = (\mathbf{I}-\mathbf{B}_r)(\mathbf{I}-\mathbf{L}_m\mathbf{M}_f)^{-1}, \quad r = f, m. \tag{13}$$

Appendix A lists the overall moduli derived from the Mori–Tanaka model for interface separation promoted either by transverse debonding/sliding or longitudinal sliding.

2.3.2. Periodic array models

Under overall uniform fields applied to a periodic approximation of the actual material microgeometry, a unit cell that is representative of the composite lamina can be selected for evaluation of the local fields and overall response (Iwakuma and Nemat-Nasser, 1983; Dvorak and Teply, 1985; Nemat-Nasser and Hori, 1993; Michel et al., 1999). In this case, the subdivisions V_r, $r = 1, 2, \ldots, Q$, represent finite volumes which belong either to the matrix or to the fiber. The stress and strain are assumed to be uniform within each subvolume. In the present work, we represent the microgeometry of a fibrous lamina in the transverse plane by a periodic hexagonal dispersion of the fibers (Dvorak and Teply, 1985). Fig. 1b shows the idealized transverse plane and the smallest RVE that can be selected for evaluation of the local fields. A 3D view of the RVE is shown in Fig. 2a, and a sample subdivision into finite elements is given in Fig. 2b.

The overall response and the piecewise uniform local stresses and strains in the subvolumes caused by a uniform stress increment $\dot{\bar{\boldsymbol{\sigma}}}$, or strain increment $\dot{\bar{\boldsymbol{\varepsilon}}}$, can be either evaluated from Eqs. (4)–(6), or computed with a finite element analysis of the representative volume.

In the finite element evaluation, the representative volume is supported against rigid body motion as shown in Fig. 2a and subjected to nodal forces, which equilibrate the overall stress rates. Assuming a linear displacement field for an equivalent, macroscopically homogeneous RVE, the nodal forces, $\dot{\mathbf{p}}_k$, $k = 1, 2, \ldots, 6$, applied at the independent degrees of freedom, Fig. 2a, are derived as (Bahei-El-Din et al., 1998)

$$\begin{aligned} &\dot{p}_1 = -\frac{H}{\xi}\dot{\bar{\sigma}}_{22}, \quad \dot{p}_2 = -\frac{H}{\xi}\dot{\bar{\sigma}}_{23}, \quad \dot{p}_3 = -\frac{H\xi}{2}\dot{\bar{\sigma}}_{33} + \frac{H}{2\xi}\dot{\bar{\sigma}}_{23} - \frac{1}{2}\dot{\bar{\sigma}}_{31}, \\ &\dot{p}_4 = \frac{H\xi}{2}\dot{\bar{\sigma}}_{33} + \frac{H}{2\xi}\dot{\bar{\sigma}}_{23} - \frac{1}{2}\dot{\bar{\sigma}}_{31}, \quad \dot{p}_5 = \dot{\bar{\sigma}}_{11}, \quad \dot{p}_6 = \dot{\bar{\sigma}}_{12}, \end{aligned} \tag{14}$$

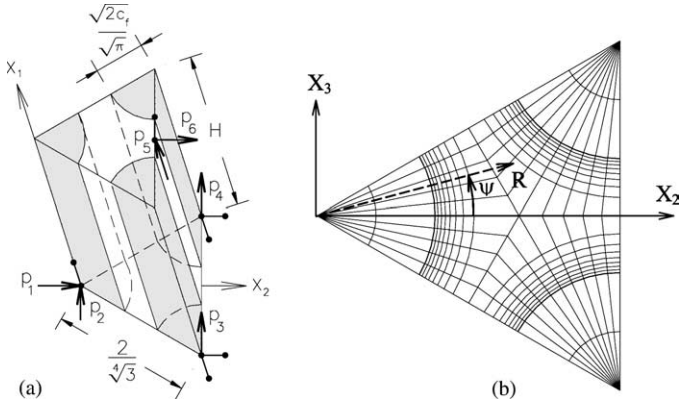

Fig. 2. RVE of a hexagonal array model, (a) geometry and boundary conditions, and (b) finite element mesh in the transverse plane.

where $\xi = \sqrt[4]{3}$, and H is the length of the unit cell in the axial direction $\bar{x}_1$. Multipoint constraints derived from the assumed periodic geometry of the microstructure are applied at the boundary of the representative volume together with generalized plane strain boundary conditions (Teply and Dvorak, 1988). Time history of the local fields and overall strains are then given by an iterative finite element solution (Bahei-El-Din, 1996).

If on the other hand, Eqs. (4)–(6) are employed, the representative volume is treated as an aggregate of subvolumes V_r, $r = 1, 2, \ldots, Q$, with concentration factors $\mathbf{A}_r$, $\mathbf{B}_r$, and transformation influence functions, $\mathbf{D}_{rs}$, $\mathbf{F}_{rs}$, $r, s = 1, 2, \ldots, Q$, which depend on the selected microgeometry and the local properties. Considering the hexagonal array model, the required factors are determined from finite element analysis of the representative volume in Fig. 2 under nodal forces which represent certain overall stress components. For example, the kth column, $k = 1, 2, \ldots, 6$, of the stress concentration matrix $\mathbf{B}_r$, $r = 1, 2, \ldots, Q$, is given by the stresses caused in V_r by an overall stress component $\sigma_k = 1$, as suggested by Eq. $(4)_2$.

Similarly, Eq. $(4)_1$ suggests that the kth column, $k = 1, 2, \ldots, 6$, of the transformation matrix, $\mathbf{D}_{rs}$, $r, s = 1, 2, \ldots, Q$, represents the strains caused in subvolume V_r by a transformation strain $\mu_k = 1$ applied to V_s, while the unit cell is fully constrained. The equivalent nodal forces are given by (Bahei-El-Din, 1996) $\mathbf{p} = -V_s \mathbf{\Lambda}^{\mathrm{T}} \mathbf{L}_s \boldsymbol{\mu}_s$, where $\mathbf{\Lambda}$ relates nodal displacements and element strains and $\boldsymbol{\mu}_s$ is the transformation strain vector applied to V_s. A total of $6Q$ similar problems are to be solved to compute all six columns of the transformation influence functions. However, internal symmetry of the unit cell in the transverse plane can be utilized to simplify this process (Dvorak et al., 1994). Evaluation of the stress influence functions $\mathbf{F}_{rs}$ follows a similar procedure in which a unit transformation stress component $\lambda_k = 1$, $k = 1, 2, \ldots, 6$, is applied to V_s.

In the absence of local damage, the concentration factors and transformation influence functions are constant, and are computed prior to the analysis of the RVE. On the other hand, changes in the local stiffness of the subvolumes due to damage require re-evaluation of all the factors in the course of the numerical solution of Eqs. (4)–(6). In this case, evaluation of the local fields and overall strains using a full finite element solution of the RVE as described earlier can be more efficient.

With the element stresses determined along the loading path, the onset of local damage in the form of debonding and/or sliding along the fiber/matrix interface is evaluated by comparing the resolved stresses in the matrix interface elements to the interface strength magnitudes. Referring to the cylindrical coordinate system shown in Fig. 2b, and accounting for friction, the onset of fiber debonding caused in the transverse plane by the radial traction component is characterized by

$$\sigma_{RR} \equiv \max \left\{ \sigma_{RR}^{(r)} \right\}_{r=1,2,\ldots,Q^\circ} = \sigma_{ult}, \tag{15}$$

where Q° denotes the number of matrix elements at the fiber interface. Sliding at the interface in the transverse plane is caused by the tangential traction component and is characterized by

$$\sigma_{R\Psi} \equiv \max \left\{ \begin{array}{ll} |\sigma_{R\Psi}^{(r)}| & \text{if } \sigma_{RR}^{(r)} \geqslant 0 \\ |\sigma_{R\Psi}^{(r)}| + \upsilon \sigma_{RR}^{(r)} & \text{if } \sigma_{RR}^{(r)} < 0 \end{array} \right\}_{r=1,2,\ldots,Q^\circ} = \tau_{ult}, \tag{16}$$

where υ is coefficient of friction. The resolved radial and shear tractions are given by

$$\begin{aligned} \sigma_{RR}^{(r)} &= \sigma_{22}^{(r)} \cos^2 \psi_r + \sigma_{33}^{(r)} \sin^2 \psi_r + \sigma_{23}^{(r)} \sin 2\psi_r, \\ \sigma_{R\Psi}^{(r)} &= \frac{1}{2} \left(\sigma_{33}^{(r)} - \sigma_{22}^{(r)} \right) \sin 2\psi_r + \sigma_{23}^{(r)} (\cos^2 \psi_r - \sin^2 \psi_r). \end{aligned} \tag{17}$$

The onset of sliding in the longitudinal plane is determined by the equality

$$\sigma_{1R} \equiv \max \left\{ \begin{array}{ll} |\sigma_{1R}^{(r)}| & \text{if } \sigma_{RR}^{(r)} \geqslant 0 \\ |\sigma_{1R}^{(r)}| + \upsilon \sigma_{RR}^{(r)} & \text{if } \sigma_{RR}^{(r)} < 0 \end{array} \right\}_{r=1,2,\ldots,Q^\circ} = \tau_{ult}, \tag{18}$$

where the resolved longitudinal shear stress in the interface elements is written as

$$\sigma_{1R}^{(r)} \equiv \sigma_{31}^{(r)} \sin\psi_r + \sigma_{12}^{(r)} \cos\psi_r. \tag{19}$$

At the onset of interface debonding by one or more of the failure criteria given by Eqs. (15), (16) or (18), in Q^* matrix interface elements, certain stress tractions cannot be transmitted across the interface and must be released and redistributed at an overall stress increment $\dot{\bar{\boldsymbol{\sigma}}} = \mathbf{0}$. The corresponding stresses described in the lamina coordinate system are given by Eq. (7) in terms of matrix $\boldsymbol{\Phi}_\rho$, $\rho \in Q^*$. Moreover, the local stiffness matrix must be modified to reflect inability of the affected interface elements to support certain stress components under subsequent loading. Appendix B lists these matrices for each of the damage criteria given by Eqs. (15), (16) and (18).

3. Analysis of a symmetric laminate

3.1. Governing equations

We now consider a symmetric laminated plate consisting of $2N$ fully bonded thin elastic plies, Fig. 3, subjected to mechanical loads. Referred to a Cartesian coordinate system, x_j, $j = 1, 2, 3$, in which the x_1x_2-plane coincides with the midplane of the laminate, in-plane membrane forces and the corresponding uniform stresses, σ_{11}, σ_{22}, and σ_{12} are applied, together with a uniform normal stress σ_{33}, in the thickness direction x_3. The out-of-plane normal stress, which might be combined with the in-plane loads, is found, for example, in fabrication by isostatic pressing, and in pressure vessels. Let $\dot{\boldsymbol{\sigma}} = [\dot{\sigma}_{11}, \dot{\sigma}_{22}, \dot{\sigma}_{12}]$ lists the in-plane stress rates applied to the laminate, and $\dot{\boldsymbol{\varepsilon}} = [\dot{\varepsilon}_{11}, \dot{\varepsilon}_{22}, 2\dot{\varepsilon}_{12}]$ lists the corresponding strain rates. The latter are caused by the applied stresses, $\dot{\boldsymbol{\sigma}}$ and $\dot{\sigma}_{33}$, and any transformation strains, or stresses, generated in the individual plies, such as stresses released due to local damage.

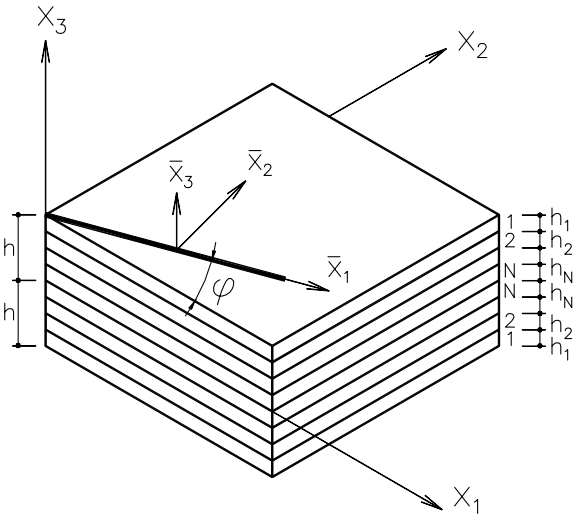

Fig. 3. Geometry of a symmetric laminate.

Hence, time rates of the laminate in-plane stresses and strains are related by (Bahei-El-Din, 1992),

$$\dot{\boldsymbol{\sigma}} = \mathbf{L}\dot{\boldsymbol{\varepsilon}} + \mathbf{k}\dot{\sigma}_{33} + \dot{\boldsymbol{\lambda}}, \tag{20}$$

$$\dot{\boldsymbol{\varepsilon}} = \mathbf{M}\dot{\boldsymbol{\sigma}} + \mathbf{f}\dot{\sigma}_{33} + \dot{\boldsymbol{\mu}}, \tag{21}$$

where $\dot{\boldsymbol{\lambda}} = [\dot{\lambda}_{11}, \dot{\lambda}_{22}, \dot{\lambda}_{12}]$ and $\dot{\boldsymbol{\mu}} = [\dot{\mu}_{11}, \dot{\mu}_{22}, 2\dot{\mu}_{12}]$ are in-plane transformation stress and strain, respectively, $\mathbf{L}$ and $\mathbf{M}$ are the elastic stiffness and compliance matrices for in-plane loading, $\mathbf{k}$ lists the in-plane stresses caused by a unit out-of-plane stress, $\sigma_{33} = 1$, in the absence of $\boldsymbol{\varepsilon}$ and $\boldsymbol{\lambda}$, and $\mathbf{f}$ is the elastic compliance associated with the out-of-plane normal stress. From (20) and (21), there is $\mathbf{L} = \mathbf{M}^{-1}$, $\mathbf{k} = -\mathbf{L}\mathbf{f}$, $\boldsymbol{\lambda} = -\mathbf{L}\boldsymbol{\mu}$.

In analogy with (20) and (21), the uniform in-plane stress and strain rates of a ply (i), $i = 1, 2, \ldots, N$, in the local coordinate system $\bar{x}_j$, $j = 1, 2, 3$, Fig. 3, can be written as,

$$\dot{\bar{\tilde{\boldsymbol{\sigma}}}}_i = \overline{\widetilde{\mathbf{L}}}_i \dot{\bar{\tilde{\boldsymbol{\varepsilon}}}}_i + \bar{\mathbf{k}}_i \dot{\bar{\sigma}}_{33}^{(i)} + \dot{\bar{\tilde{\boldsymbol{\lambda}}}}_i, \tag{22}$$

$$\dot{\bar{\tilde{\boldsymbol{\varepsilon}}}}_i = \overline{\widetilde{\mathbf{M}}}_i \dot{\bar{\tilde{\boldsymbol{\sigma}}}}_i + \bar{\mathbf{f}}_i \dot{\bar{\sigma}}_{33}^{(i)} + \dot{\bar{\tilde{\boldsymbol{\mu}}}}_i. \tag{23}$$

Here, symbols decorated with a top tilde ($\sim$) indicate quantities associated with in-plane loads. Matrices $\overline{\widetilde{\mathbf{L}}}_i$ and $\overline{\widetilde{\mathbf{M}}}_i = \overline{\widetilde{\mathbf{L}}}_i^{-1}$ are elastic stiffness and compliance matrices, $\bar{\mathbf{k}}_i$ and $\bar{\mathbf{f}}_i = -\overline{\widetilde{\mathbf{M}}}_i \bar{\mathbf{k}}_i$ are in-plane stress and strain caused in the ply by a unit out-of-plane normal stress, and $\bar{\tilde{\boldsymbol{\mu}}}_i$ and $\bar{\tilde{\boldsymbol{\lambda}}}_i = -\overline{\widetilde{\mathbf{L}}}_i \bar{\tilde{\boldsymbol{\mu}}}_i$ are in-plane transformation strain and stress. To make the connection between the equations derived in Section 2 and the equations derived here, we write the lamina in-plane stress and strain vectors $\bar{\tilde{\boldsymbol{\sigma}}}_i$, $\bar{\tilde{\boldsymbol{\varepsilon}}}_i$, and the out-of-plane stress $\bar{\sigma}_{33}^{(i)}$ in terms of the full, six-dimensional stress and strain vectors $\bar{\boldsymbol{\sigma}}_i$, $\bar{\boldsymbol{\varepsilon}}_i$ as

$$\bar{\tilde{\boldsymbol{\sigma}}}_i = \mathscr{I}^{\mathrm{T}} \bar{\boldsymbol{\sigma}}_i, \quad \mathscr{I} = [\, \imath_1 \quad \imath_2 \quad \imath_6 \,], \quad \bar{\sigma}_{33}^{i} = \imath_3^{\mathrm{T}} \bar{\boldsymbol{\sigma}}_i, \tag{24}$$

where $\imath_k$ is a column vector of order (6×1) with the kth entry equals one, and null entries otherwise.

The overall stiffness matrices $\widetilde{\mathbf{L}}_i$ and $\bar{\mathbf{k}}_i$ of a transversely isotropic lamina are given by (Bahei-El-Din, 1992)

$$\overline{\widetilde{\mathbf{L}}}_i = \frac{1}{k+m}\begin{bmatrix} E_L k + mn & 2m\ell & 0 \\ 2m\ell & 4km & 0 \\ 0 & 0 & p(k+m) \end{bmatrix} = \overline{\widetilde{\mathbf{M}}}_i^{-1}, \quad \bar{\mathbf{k}}_i = \frac{1}{k+m}\begin{bmatrix} \ell \\ k-m \\ 0 \end{bmatrix}, \tag{25}$$

where E_L is the overall longitudinal Young's modulus, and k, ℓ, m, n, p are Hill's (1964) moduli. The latter are related to the engineering moduli by $E_L = n - \ell^2/k$, $\nu_L = \ell/2k$, $m = G_T = E_T/2(1+\nu_T)$, $G_L = p$, where E_T is transverse Young's modulus, ν_L is Poisson's ratio associated with longitudinal straining, and G_L, G_T are longitudinal and transverse shear moduli.

When expressed in the overall coordinate system x_j, $j = 1, 2, 3$, Eqs. (22) and (23) are written as

$$\dot{\tilde{\boldsymbol{\sigma}}}_i = \widetilde{\mathbf{L}}_i \dot{\tilde{\boldsymbol{\varepsilon}}}_i + \mathbf{k}_i \dot{\sigma}_{33}^{(i)} + \dot{\tilde{\boldsymbol{\lambda}}}_i, \tag{26}$$

$$\dot{\tilde{\boldsymbol{\varepsilon}}}_i = \widetilde{\mathbf{M}}_i \dot{\tilde{\boldsymbol{\sigma}}}_i + \mathbf{f}_i \dot{\sigma}_{33}^{(i)} + \dot{\tilde{\boldsymbol{\mu}}}_i, \tag{27}$$

where (Bahei-El-Din, 1992)

$$\bar{\tilde{\boldsymbol{\sigma}}}_i = \mathbf{R}_i \tilde{\boldsymbol{\sigma}}_i, \quad \bar{\sigma}_{33}^{i} = \sigma_{33}^{i}, \quad \bar{\tilde{\boldsymbol{\varepsilon}}}_i = \mathbf{N}_i \tilde{\boldsymbol{\varepsilon}}_i, \tag{28}$$

$$\bar{\tilde{\boldsymbol{\lambda}}}_i = \mathbf{R}_i \tilde{\boldsymbol{\lambda}}_i, \quad \bar{\tilde{\boldsymbol{\mu}}}_i = \mathbf{N}_i \tilde{\boldsymbol{\mu}}_i, \quad \tilde{\boldsymbol{\lambda}}_i = -\overline{\mathbf{L}}_i \bar{\tilde{\boldsymbol{\mu}}}_i, \tag{29}$$

$$\widetilde{\mathbf{L}}_i = \mathbf{N}_i^{\mathrm{T}} \overline{\widetilde{\mathbf{L}}}_i \mathbf{N}_i = \widetilde{\mathbf{M}}_i^{-1}, \quad \mathbf{k}_i = \mathbf{N}_i^{\mathrm{T}} \bar{\mathbf{k}}_i = -\widetilde{\mathbf{L}}_i \mathbf{f}_i, \tag{30}$$

$$\mathbf{R}_i^{\mathrm{T}} = \mathbf{N}_i^{-1} = \begin{bmatrix} \cos^2\varphi_i & \sin^2\varphi_i & -\frac{1}{2}\sin 2\varphi_i \\ \sin^2\varphi_i & \cos^2\varphi_i & \frac{1}{2}\sin 2\varphi_i \\ \sin 2\varphi_i & -\sin 2\varphi_i & \cos 2\varphi_i \end{bmatrix}, \quad \mathbf{N}_i = \begin{bmatrix} \cos^2\varphi_i & \sin^2\varphi_i & \frac{1}{2}\sin 2\varphi_i \\ \sin^2\varphi_i & \cos^2\varphi_i & -\frac{1}{2}\sin 2\varphi_i \\ -\sin 2\varphi_i & \sin 2\varphi_i & \cos 2\varphi_i \end{bmatrix}, \tag{31}$$

and φ_i is the angle between the local $\bar{x}_1$-axis and the overall x_1-axis, Fig. 3.

In general, six transformation stress components can occur in a lamina. However, only the in-plane components $\tilde{\boldsymbol{\lambda}}_i = [\lambda_{11}, \lambda_{22}, \lambda_{12}]$ cause in-plane stresses in the perfectly bonded plies. The out-of-plane transformation strains caused in the plies can be accommodated without introducing additional in-plane stresses in the plies. Hence, the lamina stresses due to the in-plane stress $\dot{\boldsymbol{\sigma}}$ and the out-of-plane normal stress $\dot{\sigma}_{33}$ applied to the laminate, and the lamina transformation stresses are written as the sum of the individual contributions (Dvorak and Bahei-El-Din, 1995),

$$\dot{\tilde{\boldsymbol{\sigma}}}_i = \mathbf{H}_i\dot{\boldsymbol{\sigma}} + \boldsymbol{\kappa}_i\dot{\sigma}_{33} + \sum_{j=1}^{N}\mathbf{K}_{ij}\dot{\tilde{\boldsymbol{\lambda}}}_j, \quad \dot{\sigma}_{33}^{(i)} = \dot{\sigma}_{33}, \quad i = 1, 2, \ldots, N. \tag{32}$$

Matrices $\mathbf{H}_i$ and $\boldsymbol{\kappa}_i$ are stress distribution factors for in-plane overall stresses, and out-of-plane normal stress, respectively, $\mathbf{K}_{ij}$ is a transformation influence function, and

$$\mathbf{H}_i = \widetilde{\mathbf{L}}_i\mathbf{L}^{-1}, \quad \boldsymbol{\kappa}_i = \widetilde{\mathbf{L}}_i(\mathbf{f} - \mathbf{f}_i), \quad \mathbf{L} = \sum_{i=1}^{N} c_i\widetilde{\mathbf{L}}_i, \quad \mathbf{f} = -\mathbf{L}^{-1}\boldsymbol{\kappa}, \tag{33}$$

$$\boldsymbol{\kappa} = \sum_{i=1}^{N} c_i\boldsymbol{\kappa}_i, \quad \mathbf{K}_{ij} = \delta_{ij}\mathbf{I} - c_j\mathbf{H}_i, \quad \sum_{i=1}^{N} c_i\mathbf{H}_i = \mathbf{I}, \quad \sum_{i=1}^{N} c_i\boldsymbol{\kappa}_i = \mathbf{0}, \tag{34}$$

where $c_i = h_i/h$ is thickness fraction, h is half the laminate thickness, h_i is the lamina thickness, δ_{ij} is the Kronecker's tensor, $\mathbf{I}$ is identity matrix, and $\mathbf{0}$ is a null vector. From (6), (24) and (28), the in-plane transformation stress $\tilde{\boldsymbol{\lambda}}_i$ is given for lamina (i) by

$$\tilde{\boldsymbol{\lambda}}_i = \mathbf{N}^{\mathrm{T}}\mathscr{I}^{\mathrm{T}}\sum_{r=1}^{Q_i} c_r\mathbf{A}_r^{\mathrm{T}}\dot{\boldsymbol{\lambda}}_r, \tag{35}$$

where Q_i is the number of subvolumes in lamina (i).

With the lamina stresses now provided in the laminate coordinate system by (32), and in the lamina coordinates by the transformation rule $(28)_1$, we can proceed to determine the stresses in subvolumes $V_r^{(i)}$, $r = 1, 2, \ldots, Q_i$, for all plies, $i = 1, 2, \ldots, N$. If a finite element solution is sought in a representative volume of the lamina (Section 2.3), Eq. (14) is used to determine the nodal forces caused by the lamina stresses $\bar{\boldsymbol{\sigma}}_i = [\bar{\sigma}_{11}, \bar{\sigma}_{22}, \bar{\sigma}_{33}, 0, 0, \bar{\sigma}_{12}]_{(i)}$. On the other hand, local stresses in the subvolumes can be written in terms of the laminate applied stresses by substituting (33) into $(5)_2$ and utilizing (25) and (29). The result is

$$\dot{\boldsymbol{\sigma}}_r^{(i)} = [\mathbf{B}_r\mathscr{I}\mathbf{R}_i\mathbf{H}_i]\dot{\boldsymbol{\sigma}} + [\mathbf{B}_r(\mathscr{i}_3 + \mathscr{I}\mathbf{R}_i\boldsymbol{\kappa}_i)]\dot{\sigma}_{33} + \mathbf{B}_r\mathscr{I}\mathbf{R}_i\sum_{j=1}^{N}\left(\mathbf{K}_{ij}\mathbf{N}_j^{\mathrm{T}}\mathscr{I}^{\mathrm{T}}\sum_{r=1}^{Q_j} c_r\mathbf{A}_r^{\mathrm{T}}\dot{\boldsymbol{\lambda}}_r^{(j)}\right) + \sum_{s=1}^{Q_i}\left(\mathbf{F}_{rs}^{(i)}\dot{\boldsymbol{\lambda}}_s^{(i)}\right). \tag{36}$$

The first and second terms in (36) provide, respectively, the local stress caused by the overall in-plane stresses and out-of-plane normal stress applied to the laminate. The last two terms of Eq. (36) represent the local stresses caused in subvolumes of lamina (i) by transformation stresses found in the subvolumes of all plies. These represent two effects: one due to the constraints induced by the subvolumes in lamina (i), and one due to the in-plane equi-strain condition imposed on the plies.

3.2. Damage-induced transformation stress

In Section 2.2, we considered interface damage in a single lamina and provided certain stress criteria which signal failure by debonding and/or sliding using two micromechanical models in Section 2.3. Here, we consider a symmetric laminate with damage in one or more plies and determine how this affects the local stresses in all plies.

Let $t = t^*$ indicate the onset of damage in $Q_\eta^* < Q_\eta$ subvolumes in lamina $\eta = 1, 2, \ldots, P \leqslant N$, where Q_η is the number of subvolumes in lamina η. For each such lamina, certain stress components, provided by Eq. (7), in subvolumes V_ρ, $\rho = 1, 2, \ldots, Q_\eta^*$, are released instantaneously and redistributed simultaneously at a constant overall stress. Hence, at $t = t^{*+}$, immediately after the onset of damage, there is $\dot{\boldsymbol{\sigma}} = \mathbf{0}$, $\dot{\sigma}_{33} = 0$. At this instant, the released stresses are treated as transformation stresses in the affected subvolumes. When these are substituted into (36), the local stresses caused instantaneously in all subvolumes V_r, $r = 1, 2, \ldots, Q_i$, of all plies $i = 1, 2, \ldots, N$ can be found. The accumulated stress in the subvolumes at $t = t^*$ is then updated as

$$\boldsymbol{\sigma}_r^{(i)}(t^{*+}) = \boldsymbol{\sigma}_r^{(i)}(t^*) - \mathbf{B}_r \mathscr{I} \mathbf{R}_i \sum_{\eta=1}^{P} \left(\mathbf{K}_{i\eta} \mathbf{N}_\eta^{\mathrm{T}} \mathscr{I}^{\mathrm{T}} \sum_{\rho=1}^{Q_\eta^*} c_\rho \mathbf{A}_\rho^{(\eta)^{\mathrm{T}}} \boldsymbol{\Phi}_\rho^{(\eta)} \boldsymbol{\sigma}_\rho^{(\eta)}(t^*) \right) - \delta_{i\eta} \sum_{\rho=1}^{Q_i^*} \mathbf{F}_{r\rho}^{(i)} \boldsymbol{\Phi}_\rho^{(i)} \boldsymbol{\sigma}_\rho^{(i)}(t^*). \tag{37}$$

We note that the last term is the self-induced stress caused in the subvolumes of lamina (i) by interface damage found in the same lamina.

4. Implementation and application

To recapitulate, analysis of fibrous laminates with damage evolution at the fiber/matrix interface in the individual plies was described in terms of two material scales with coupled equations. One material scale represents the macroscopic behavior of the laminate under in-plane mechanical loads, and the other material scale represents the micromechanical behavior of unidirectional composites. In implementing this procedure, the local, piecewise uniform fields in the subvolumes of the RVE of a unidirectional composite were computed with the finite element method as outlined in Section 2.3.2. The elastic module of the Viscopac program developed by Bahei-El-Din (1996) was modified to simulate damage in the matrix elements located at the fiber interface. As described in Section 2.3.2, this method centers on modifying the local stiffness for the damaged elements, and redistribution of the affected stress components by applying equivalent nodal forces. Results obtained from this procedure using the mesh of Fig. 2b are described in this section. For comparison with predictions of fully debonded averaging models, results obtained with the Mori–Tanaka model are also shown for some applications.

4.1. Comparison with experiments

The experiments of Ghosh et al. (2000) provide the stress–strain response of a unidirectional composite loaded in the transverse direction. The fibers are stainless steel filaments with a diameter of 2.36 mm, Young's modulus $E = 210$ GPa, and Poisson's ratio $v = 0.3$. The matrix is an epoxy resin with $E = 4.6$ GPa, and $v = 0.4$. The experimental results are provided for two specimens, one with a single fiber, and one with five fibers. The fiber volume fraction was in the order of 10.7% for the specimen of one fiber, and 1.14% for the specimen with five fibers.

Our simulation utilized the RVE model of Fig. 1b. Consequently the model represents a composite with multiple fibers, and as such is expected to be more representative of the five-fiber specimen tested by Ghosh et al. (2000). Fig. 4 compares the computed and the measured response for the steel/epoxy composite under

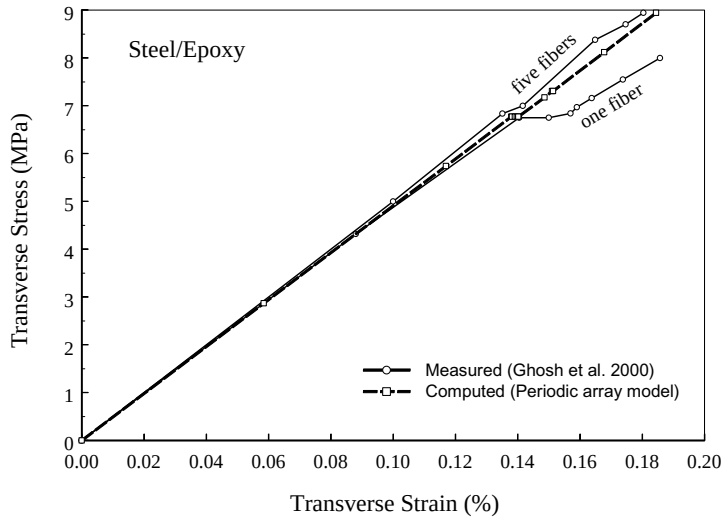

Fig. 4. Comparison of model predictions and experimental measurements for the stress–strain response of a unidirectional composite subjected to transverse loading.

transverse loading. In the linear range, before the onset of interface debonding, the overall response is dominated by the matrix behavior since the fiber volume fraction in either specimen is small. The computed response matched the measured response in the linear range when the fiber volume content was set at 8%. The onset of interface damage occurs in both specimens at an overall stress of 6.8 MPa, and causes a sudden increase in overall strain, which is substantially larger in the specimen with one fiber than the specimen with five fibers.

In the simulation, the magnitude of σ_{ult}, the interface normal bond strength, was determined from the local maximum normal stress found in the matrix interface elements in direction of the fiber radius at an overall stress of 6.8 MPa. The magnitude of σ_{ult} was found as 9.5 MPa, which was then applied throughout the analysis. The model predictions at, and beyond the onset of interface debonding agree with the experimental measurements for the specimen with five fibers, Fig. 4. At the onset of interface debonding, the stresses released from the interface elements in the RVE model lead to a plateau in the stress–strain curve as shown in Fig. 4, a behavior which is also observed in the experiments.

4.2. Examples

Several examples are described here to illustrate the model predictions for composite laminates under in-plane loads. The results were obtained for a glass ceramic matrix (CAS), reinforced with a silicon-carbide fiber at 39% (Wooh and Daniel, 1994). The elastic moduli of the SiC fiber are assumed as $E = 170$ GPa, and $v = 0.25$. The elastic moduli of the matrix were back calculated by matching the overall moduli given by the Mori–Tanaka averaging model with their counterparts, which were measured by Wooh and Daniel (1994). The elastic moduli of the CAS matrix were computed as $E = 98$ GPa, and $v = 0.135$. The strength of the fiber/matrix interface was assumed as 50 MPa under debonding, and 80 MPa under sliding. A coefficient of friction of 0.3 was also assumed at the interface.

The response of a unidirectional composite under off-axis, normal stress is shown in Fig. 5. The predictions from the periodic array model are shown for loading in the fiber direction, 0°, the transverse direction, 90°, and at several intermediate angles. The response under transverse loading as predicted with the Mori–Tanaka averaging model is also shown in Fig. 5. The periodic array model provided an overall

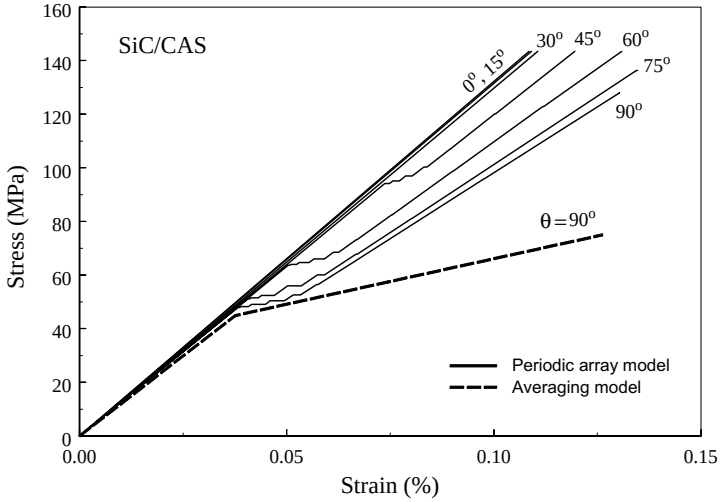

Fig. 5. Model predictions for the stress–strain response of a unidirectional composite subjected to off-axis loading.

elastic Young's modulus $E_L = 132$ GPa in the longitudinal direction, and $E_T = 126$ GPa in the transverse direction. The Mori–Tanaka estimate under transverse loading is $E_T = 120$ GPa. It is seen that the loading direction has a small effect on the overall elastic stiffness. This is expected since the ratio of Young's moduli of the fiber and the matrix is 1.73, while the ratio of their volume fraction is 0.63. We note that a simple rule of mixture based on equi-strain in the longitudinal direction of a unidirectional composite, and equi-stress in the transverse direction provides $E_L = 126$ GPa and $E_T = 117$ GPa. Hence the contributions of the fiber and the matrix to the overall stiffness are approximately equal in all directions when they are fully bonded.

Up to an overall load of 170 MPa, the composite plies loaded in the fiber direction, and at 15° did not exhibit failure in any of the matrix elements located at the fiber interface. Loading at a larger off-axis angle causes the interface to debond and/or slide. Under the interface strength magnitudes listed above, interface failure was due to fiber sliding in the 30° ply, and due to fiber debonding in the plies loaded at an angle $\geqslant 45°$. Since the elastic response under all loading directions is almost identical, the changes seen in Fig. 5 in the overall stiffness beyond the onset of interface failure reflect only the effect of damage on the overall response. This effect is also shown in Fig. 6 where the damage strain, computed as the difference between the overall strain and the elastic strain, is plotted versus the applied stress.

The overall stress at the onset of interface debonding decreases as the direction of the applied overall stress deviates more from the fiber direction. As seen in Figs. 5 and 6, progressive failure in the interface elements cause sudden, successive increases in the overall strain. Moreover, these results suggest that the length of the fiber/matrix interface arc, which sustains failure by debonding increases as the off-axis loading angle increases. For the element subdivision shown in Fig. 2b, damage saturation is reached for a center angle of the debonded interface arc of 120°. At damage saturation, the overall stiffness computed with the periodic array model under transverse loading is 98 GPa. On the other hand, the Mori–Tanaka solution for a porous matrix, which represents a fully debonded fiber, predicts a transverse modulus of 34 GPa. For comparison, we evacuated all matrix elements in the thin interface layer in the mesh of Fig. 2b and computed the transverse modulus as 23 GPa. Hence, the ratio of the Mori–Tanaka estimate of the transverse elastic modulus of a unidirectional composite to that given by the periodic array model is 1.48 for a fully debonded fiber, but only 0.95 for a fully bonded interface.

The overall response of a quasi-isotropic, (0/±45/90) symmetric laminate caused by an overall stress applied in direction of the 0° ply is shown in Figs. 7 and 8. The results predicted by the periodic array RVE

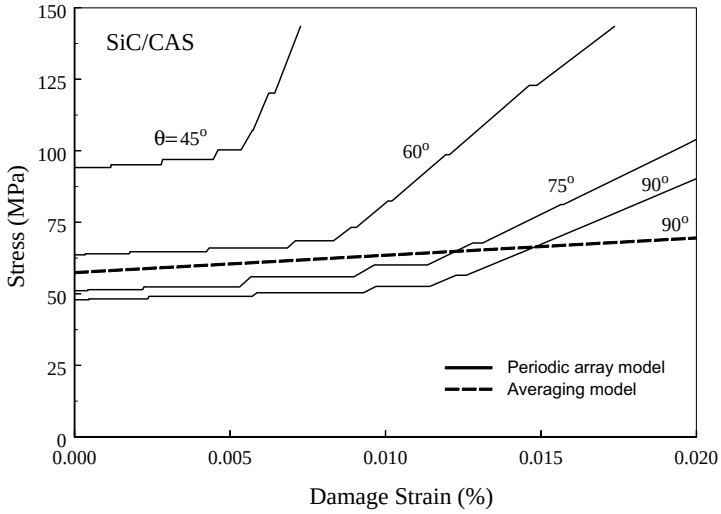

Fig. 6. Model predictions for the stress–damage strain response of a unidirectional composite subjected to off-axis loading.

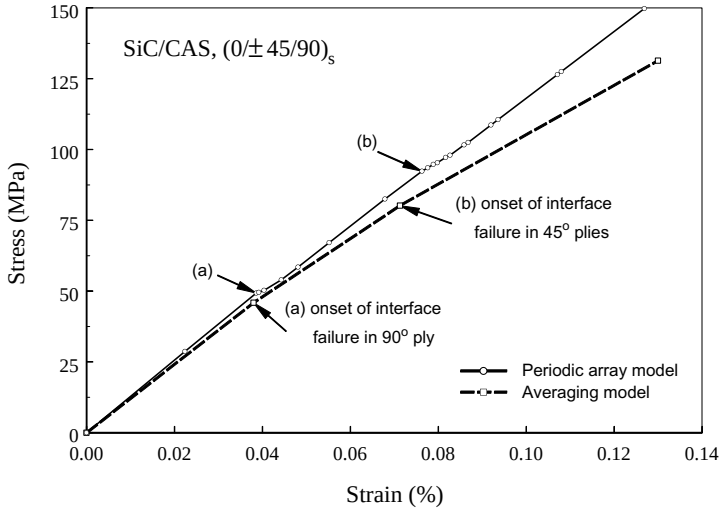

Fig. 7. Model predictions for the stress–strain response of a composite laminate subjected to a normal stress in direction of the 0° ply.

model, Fig. 2, and by the averaging model are shown. Initial failure is detected in the 90° ply due to exceeding the ultimate normal strength at the interface. While the fiber in the averaging model debonds at the entire fiber circumference, progressive debonding occurs in the RVE model. This is illustrated in Fig. 9, which shows the evolution of damage in the 90° ply as the overall load applied to the laminate increases. It is seen that the length of the damaged fiber interface arc increases with loading, and a damage saturation state occurs at an arc center angle θ of 120°, and an overall stress of 149.79 MPa. Interface damage occurs in the off-axis, ±45° plies, also by debonding rather than sliding. This occurs simultaneously with the damage seen in the 90° ply, but initiates at a higher overall stress of 93.59 MPa, compared to 49.48 MPa for the onset of damage in the 90° ply. Fig. 10 illustrates the evolution of damage in the ±45° plies.

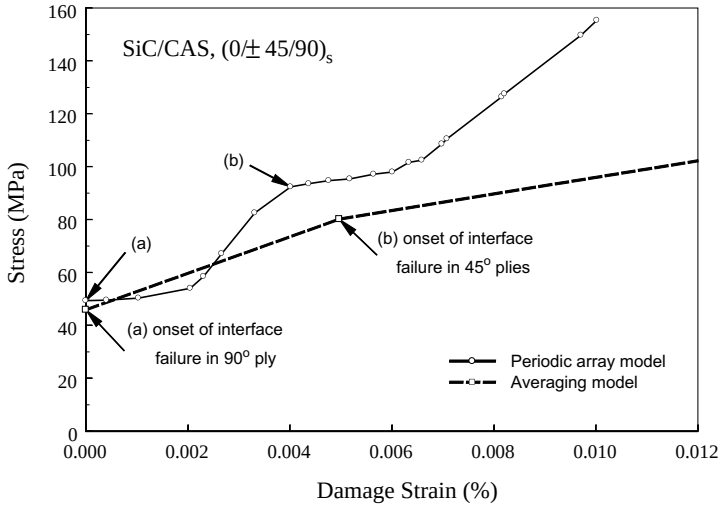

Fig. 8. Model predictions for the stress–damage strain response of a composite laminate subjected to a normal stress in direction of the 0° ply.

σ (MPa)	49.48	50.31	51.64	54.0	58.52
90° ply debonding configuration	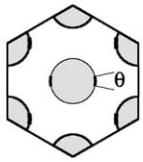	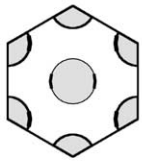	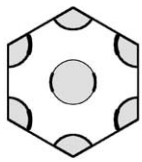	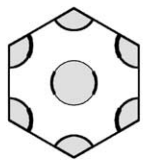	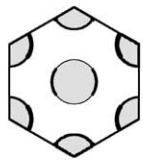
θ°	24	36	48	60	72
σ (MPa)	67.14	82.54	108.66	149.78	> 149.78
90° ply debonding configuration	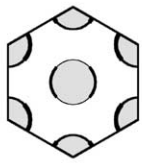	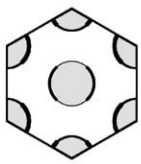	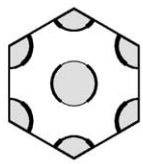	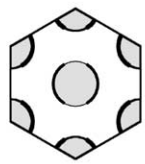	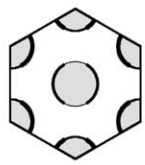
θ°	84	96	108	120	120

Fig. 9. Model predictions for the debonding configuration in the 90° ply of a SiC/CAS, $[0/\pm45/90]_s$ laminate subjected to a normal stress in direction of the 0° ply.

5. Closure

An analysis scheme for evaluation of the overall response of symmetric laminates under in-plane loads, while undergoing progressive fiber debonding in the individual plies was developed. The method is a micro/macro-mechanical analysis, which connects events at the local scale to the laminate structural scale through stress transformation factors. The solution is obtained by a coupled closed form analysis for the laminate,

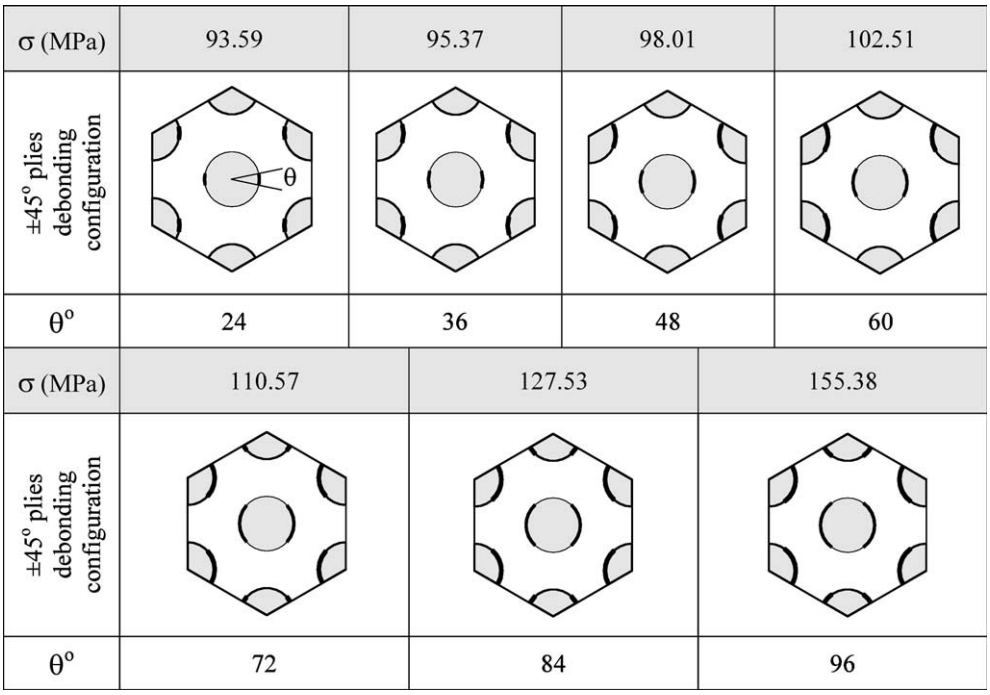

Fig. 10. Model predictions for the debonding configuration in the ±45° plies of a SiC/CAS, $[0/\pm45/90]_s$ laminate subjected to a normal stress in direction of the 0° ply.

and finite element analysis for the plies. The latter was performed for a RVE derived from an assumed hexagonal periodic array microstructure. Fiber debonding and/or sliding can take place progressively and simultaneously in the individual plies.

The onset of fiber debonding in the plies was based on a stress criterion in terms of the stresses in a small matrix volume located at the fiber interface, and resolved in the radial and tangential directions. Modifying the local stiffness associated with the affected stress components leads to stress redistribution in the RVE, and to overall transformation stresses, which cause additional stresses in the coupled plies.

The work described in this paper establishes a connection between damage initiation in the form of fiber debonding, and its progression, in a unidirectional fibrous lamina and the overall response of a laminated plate. Any micromechanical model can be utilized in the proposed analysis scheme. The periodic array model used here to describe fiber debonding and sliding represents a departure from averaging the local effects towards detailed modeling of the local stress gradients and their effect on damage progression, albeit at a higher computation cost. However, utilizing a periodic array of fibers in modeling damage implies its initiation and progression in a periodic pattern, which would not be the behavior of a real composite system where variations in the fiber spacing and interface strength are expected. An alternative is found in partially debonded or imperfect interface models, with statistical variations in the interface strength. However, solutions for this class of models at high fiber concentrations where fiber interaction is significant are not fully developed.

Finally, we note that although the focus in the present work was on fiber debonding caused by mechanical loads, the proposed analysis scheme can be utilized for other forms of local damage and applied loads. For example, matrix cracking can be modeled for the finite matrix elements in the RVE using continuum damage mechanics, and thermal strains can be easily accounted for in the lamina analysis. Also,

adopting other damage criteria for the initiation of fiber debonding in the present analysis, such as a critical energy criterion, which is known to be more suitable for small fiber volume fractions, can be easily achieved.

Appendix A

Here, we record some results related to estimates of the overall moduli of fibrous composites using averaging models. Both the fiber and matrix are assumed to be transversely isotropic with x_1 as the axis of rotational symmetry. Let E_L and E_T denote, respectively, the longitudinal and transverse elastic Young's modulus, and v_L and v_T denote Poisson's ratios under axial and transverse straining. Similarly, we denote the longitudinal and transverse elastic shear moduli by G_L and G_T. The elastic stress–strain relation $\boldsymbol{\varepsilon} = \mathbf{M}\boldsymbol{\sigma}$ for either phase, as well as for unidirectional fibrous composites, where $\mathbf{M}$ is the elastic compliance matrix, is written using the engineering moduli as

$$\begin{Bmatrix} \varepsilon_{11} \\ \varepsilon_{22} \\ \varepsilon_{33} \\ 2\varepsilon_{23} \\ 2\varepsilon_{31} \\ 2\varepsilon_{12} \end{Bmatrix} = \begin{bmatrix} 1/E_T & -v_T/E_L & -v_L/E_L & 0 & 0 & 0 \\ & 1/E_T & -v_L/E_T & 0 & 0 & 0 \\ & & 1/E_T & 0 & 0 & 0 \\ & & & 1/G_T & 0 & 0 \\ & \text{SYM.} & & & 1/G_L & 0 \\ & & & & & 1/G_L \end{bmatrix} \begin{Bmatrix} \sigma_{11} \\ \sigma_{22} \\ \sigma_{33} \\ \sigma_{23} \\ \sigma_{31} \\ \sigma_{12} \end{Bmatrix}. \tag{A.1}$$

The stiffness $\mathbf{L} = \mathbf{M}^{-1}$ is best written in terms of Hill's (1964) moduli,

$$\begin{aligned} &k = -[1/G_T - 4/E_T + 4v_L^2/E_L]^{-1}, \quad \ell = 2kv_L, \\ &n = E_L + 4kv_L^2 = E_L + \ell^2/k, \quad m = G_T, \quad p = G_L. \end{aligned} \tag{A.2}$$

The constitutive relation $\boldsymbol{\sigma} = \mathbf{L}\boldsymbol{\varepsilon}$ is then written as

$$\begin{Bmatrix} \sigma_{11} \\ \sigma_{22} \\ \sigma_{33} \\ \sigma_{23} \\ \sigma_{31} \\ \sigma_{12} \end{Bmatrix} = \begin{bmatrix} n & \ell & \ell & 0 & 0 & 0 \\ & (k+m) & (k-m) & 0 & 0 & 0 \\ & & (k+m) & 0 & 0 & 0 \\ & & & m & 0 & 0 \\ & \text{SYM.} & & & p & 0 \\ & & & & & p \end{bmatrix} \begin{Bmatrix} \varepsilon_{11} \\ \varepsilon_{22} \\ \varepsilon_{33} \\ 2\varepsilon_{23} \\ 2\varepsilon_{31} \\ 2\varepsilon_{12} \end{Bmatrix}. \tag{A.3}$$

Estimates of the overall moduli of two-phase fibrous composite materials by the Mori–Tanaka model are given by (Chen et al., 1992)

$$\begin{aligned} &p = \frac{2c_f p_m p_f + c_m(p_m p_f + p_m^2)}{2c_f p_m + c_m(p_f + p_m)}, \quad m = \frac{m_m m_f(k_m + 2m_m) + k_m m_m(c_f m_f + c_m m_m)}{k_m m_m + (k_m + 2m_m)(c_f m_m + c_m m_f)}, \\ &k = \frac{c_f k_f(k_m + m_m) + c_m k_m(k_f + m_m)}{c_f(k_m + m_m) + c_m(k_f + m_m)}, \quad \ell = \frac{c_f \ell_f(k_m + m_m) + c_m \ell_m(k_f + m_m)}{c_f(k_m + m_m) + c_m(k_f + m_m)}, \\ &n = c_m n_m + c_f n_f + (1 - c_f \ell_f - c_m \ell_m)\frac{\ell_f - \ell_m}{k_f - k_m}. \end{aligned} \tag{A.4}$$

Under interface debonding or sliding in the transverse plane, which is modeled by prescribing $E_T^f = G_T^f = 0$ (Section 2.3.1), the Mori–Tanaka overall moduli are found from (A.4) by substituting $k_f = \ell_f = m_f = 0$, $n_f = E_L^f$, and $p_f = G_L^f$. If on the other hand interface sliding occurs under longitudinal shear, the overall moduli are found from (A.4) by substituting $p_f = G_L^f = 0$.

Appendix B

Referring to the interface damage criteria given in Eqs. (15), (16) and (18) for a fibrous composite modeled with a periodic microstructure, the stresses released due to each criterion are written as shown in Eq. (7). Matrix $\mathbf{\Phi}_\rho$ is found by first transforming the current stress $\boldsymbol{\sigma}_\rho(t^*)$ to the cylindrical coordinates shown in Fig. 2b, which we denote by $\left(\widehat{x}_1, \widehat{x}_R, \widehat{x}_T\right)$, then determine which resolved stress tractions are to be released based on the above damage criteria. These tractions are then transformed back into the lamina coordinate system $(\bar{x}_1, \bar{x}_2, \bar{x}_3)$. With reference to the $\widehat{\mathbf{x}}$ coordinates, certain entries of the elastic stiffness matrix $\widehat{\mathbf{L}}_\rho$ are reduced to zero to reflect inability of the interface to transmit stresses.

For damage by radial debonding, Eq. (15), $\widehat{L}_{ij}^{(\rho)} = \widehat{L}_{ji}^{(\rho)} = 0$, $i = 2$, $j = 1, 2, \ldots, 6$, and

$$\mathbf{\Phi}_\rho = \begin{bmatrix} 0 & 0 & 0 & 0 & 0 & 0 \\ 0 & \cos^4\psi_\rho & \frac{1}{4}\sin^2 2\psi_\rho & \cos^2\psi_\rho \sin 2\psi_\rho & 0 & 0 \\ 0 & \frac{1}{4}\sin^2 2\psi_\rho & \sin^4\psi_\rho & \sin^2\psi_\rho \sin 2\psi_\rho & 0 & 0 \\ 0 & \frac{1}{2}\cos^2\psi_\rho \sin 2\psi_\rho & \frac{1}{2}\sin^2\psi_\rho \sin 2\psi_\rho & \frac{1}{2}\sin^2 2\psi_\rho & 0 & 0 \\ 0 & 0 & 0 & 0 & 0 & 0 \\ 0 & 0 & 0 & 0 & 0 & 0 \end{bmatrix}. \tag{B.1}$$

For damage by the shear sliding in the transverse plane, Eq. (16), $\widehat{L}_{ij}^{(\rho)} = \widehat{L}_{ji}^{(\rho)} = 0$, $i = 4$, $j = 1, 2, \ldots, 6$, and

$$\mathbf{\Phi}_\rho = \begin{bmatrix} 0 & 0 & 0 & 0 & 0 & 0 \\ 0 & \frac{1}{2}\sin^2 2\psi_\rho & -\frac{1}{2}\sin^2 2\psi_\rho & -\sin 2\psi_\rho \cos 2\psi_\rho & 0 & 0 \\ 0 & -\frac{1}{2}\sin^2 2\psi_\rho & \frac{1}{2}\sin^2 2\psi_\rho & \sin 2\psi_\rho \cos 2\psi_\rho & 0 & 0 \\ 0 & -\frac{1}{2}\sin 2\psi_\rho \cos 2\psi_\rho & \frac{1}{2}\sin 2\psi_\rho \cos 2\psi_\rho & \cos^2 2\psi_\rho & 0 & 0 \\ 0 & 0 & 0 & 0 & 0 & 0 \\ 0 & 0 & 0 & 0 & 0 & 0 \end{bmatrix}. \tag{B.2}$$

Under shear sliding in the longitudinal plane, Eq. (18), $\widehat{L}_{ij}^{(\rho)} = \widehat{L}_{ji}^{(\rho)} = 0$, $i = 6$, $j = 1, 2, \ldots, 6$, and

$$\mathbf{\Phi}_\rho = \begin{bmatrix} 0 & 0 & 0 & 0 & 0 & 0 \\ 0 & 0 & 0 & 0 & 0 & 0 \\ 0 & 0 & 0 & 0 & 0 & 0 \\ 0 & 0 & 0 & 0 & 0 & 0 \\ 0 & 0 & 0 & 0 & \sin^2\psi_\rho & \frac{1}{2}\sin 2\psi_\rho \\ 0 & 0 & 0 & 0 & \frac{1}{2}\sin 2\psi_\rho & \cos^2\psi_\rho \end{bmatrix}. \tag{B.3}$$

References

Bahei-El-Din, Y.A., 1992. Uniform fields, yielding, and thermal hardening in fibrous composite laminates. Int. J. Plast. 8, 867–892.

Bahei-El-Din, Y.A., 1996. Finite element analysis of viscoplastic composite materials and structures. Mech. Comp. Mater. Struct. 3, 1–28.

Bahei-El-Din, Y.A., Ibrahim, I.A., Botrous, A.G., 1998. In: Bahei-El-Din, Y.A., Dvorak, G.J. (Eds.), IUTAM Symposium on Transformation Problems in Composite and Active Materials. Kluwer Academic Publishers, Dordrecht, pp. 45–60.

Benveniste, Y., 1987. A new approach to the application of Mori–Tanaka's theory in composite materials. Mech. Mater. 6, 147–157.

Chen, T., Dvorak, G.J., Benveniste, Y., 1992. Mori–Tanaka estimates of the overall elastic moduli of certain composite materials. J. Appl. Mech. 59, 539–546.

Dvorak, G.J., 1991. Plasticity theories for fibrous composite materials. In: Everett, R.K., Arsenault, R.J. (Eds.), Metal Matrix Composites, Mechanisms and Properties, vol. 2. Academic Press, Boston, pp. 1–77.
Dvorak, G.J., 1992. Transformation field analysis of inelastic composite materials. Proc. R. Soc. Lond. A 437, 311–327.
Dvorak, G.J., Bahei-El-Din, Y.A., 1995. Transformation analysis of inelastic laminates. In: Pyrz, R. (Ed.), IUTAM Symposium on Microstructure-Property Interactions in Composite Materials. Kluwer Academic Publishers, Netherlands, pp. 89–100.
Dvorak, G.J., Benveniste, Y., 1992. On transformation strains and uniform fields in multiphase elastic media. Proc. R. Soc. Lond. A 437, 291–310.
Dvorak, G.J., Teply, J.L., 1985. Periodic hexagonal array models for plasticity analysis of composite materials. In: Sawczuk, A., Bianchi, V. (Eds.), Plasticity Today: Modelling, Methods and Applications, W. Olsazak Memorial Volume. Elsevier Scientific Publishing Co, Amsterdam, pp. 623–642.
Dvorak, G.J., Zhang, J., 2001. Transformation field analysis of damage evolution in composite materials. J. Mech. Phys. Solids 49, 2517–2541.
Dvorak, G.J., Bahei-El-Din, Y.A., Wafa, A.M., 1994. Implementation of the transformation field analysis for inelastic composite materials. Comput. Mech. 14, 201–228.
Evans, A.G., He, M.Y., Hutchinson, J.W., 1989. Interface debonding and fiber cracking in brittle matrix composites. J. Am. Ceram. Soc. 72, 2300–2303.
Eshelby, J.D., 1957. The determination of the elastic field of an ellipsoidal inclusion, and related problems. Proc. R. Soc. Lond. A 241, 376–396.
Ghosh, S., Ling, Y., Majumdar, B., Kim, R., 2000. Interfacial debonding analysis in multiple fiber reinforced composites. Mech. Mater. 32, 561–591.
Hill, R., 1963. Elastic properties of reinforced solids: some theoretical principles. J. Mech. Phys. Solids 11, 357–372.
Hill, R., 1964. Theory of mechanical properties of fibre-strengthened materials: I. Elastic behaviour. J. Mech. Phys. Solids 12, 199.
Hill, R., 1965. A self-consistent mechanics of composite materials. J. Mech. Phys. Solids 13, 213–222.
Hsueh, C.H., Becher, P.F., 1998. Interfacial shear debonding problems in fiber-reinforced ceramic composites. Acta Mater. 46, 3237–3245.
Hutchinson, J.W., Jensen, H.M., 1990. Models of fiber debonding and pullout in brittle composites with friction. Mech. Mater. 9, 139–163.
Iwakuma, T., Nemat-Nasser, S., 1983. Composites with periodic microstructure. Compos. Struct. 16, 13–19.
Levin, V.M., 1967. Thermal expansion coefficients of heterogeneous materials. Mech. Solids 11, 58–61.
Liu, Y.F., Kagawa, Y., 1996. Analysis of debonding and frictional sliding in fiber-reinforced brittle matrix composites: basic problems. Mater. Sci. Eng. A 212, 75–86.
Marshall, D.B., 1992. Analysis of fiber debonding and sliding experiments in brittle matrix composites. Acta Metall. Mater. 40, 427–441.
Michel, J.C., Moulinec, H., Suquet, P., 1999. Effective properties of composite materials with periodic microstructure: a computational approach. Comput. Meth. Appl. Mech. Eng. 172, 109–143.
Mori, T., Tanaka, K., 1973. Average stress in matrix and average elastic energy of materials with misfitting inclusions. Acta Metall. 21, 571–574.
Mumm, D.R., Faber, K.T., 1995. Interfacial debonding and sliding in brittle-matrix composites measured using an improved fiber pullout technique. Acta Metall. Mater. 43, 1259–1270.
Nemat-Nasser, S., Hori, M., 1993. Micromechanics: Overall Properties of Heterogeneous Solids. Elsevier Science Publishers, Amsterdam.
Nimmer, R.P., Bankert, R.J., Russell, E.S., Smith, G.A., Wright, P.K, 1991. Micromechanical modeling of fiber/matrix interface effects in transversely loaded SiC/Ti-6-4 metal matrix composites. J. Comp. Tech. Res. 13, 3–13.
Pochiraju, K.V., Tandon, G.P., Pagano, N.J., 2001. Analyses of single fiber pushout considering interfacial friction and adhesion. J. Mech. Phys. Solids 49, 2307–2338.
Shan, H.Z., Chou, T.W., 1995. Transverse elastic moduli of unidirectional fiber composites with fiber/matrix interfacial debonding. Comp. Sci. Tech. 53, 383–391.
Steif, P.S., Dollar, A., 1988. Longitudinal shearing of a weakly bonded fiber composite. Trans. ASME 55, 618–623.
Steif, P.S., Dollar, A., 1992. Models of fiber–matrix interfacial debonding. J. Am. Ceram. Soc. 75, 1694–1696.
Tandon, G.P., Kim, R.Y., Bechel, V.T., 2000. Evaluation of interfacial normal strength in a SCS-0/epoxy composite with cruciform specimens. Comp. Sci. Tech. 60, 2281–2295.
Teply, J.L., Dvorak, G.J., 1988. Bounds on overall instantaneous properties of elastic–plastic composites. J. Mech. Phys. Solids 36, 29–58.
Wooh, S.C., Daniel, I.M., 1994. Real-time ultrasonic monitoring of fiber–matrix debonding in ceramic–matrix composite. Mech. Mater. 17, 379–388.
Zhou, X.F., Nairn, J.A., Wagner, H.D., 1999. Fiber–matrix adhesion from the single-fiber composite test: nucleation of interfacial debonding. Composites A 30, 1387–1400.